ACS APPLIED MATERIALS & INTERFACES

www.acsami.org

Research Article

Rational Designed Mixed-Conductive Sulfur Cathodes for All-Solid-State Lithium Batteries

Jie Yue, Yonglin Huang, Sufu Liu, Ji Chen, Fudong Han,* and Chunsheng Wang*

Cite This: *ACS Appl. Mater. Interfaces* 2020, 12, 36066–36071

Read Online

ACCESS | Metrics & More | Article Recommendations | Supporting Information

ABSTRACT: All-solid-state lithium–sulfur batteries (ASSLSBs) hold great promise for safe and high-energy-density energy storage. However, developing high-performance sulfur cathodes has been proven difficult due to low electronic and ionic conductivities and large volume change of sulfur during charge and discharge. Here, we reported an approach to synthesize sulfur cathodes with a mixed electronic and ionic conductivity by infiltrating a solution consisting of Li_3PS_4 (LPS) solid electrolyte and S active material into a mesoporous carbon (CMK-3). This approach leads to a uniform dispersion of amorphous Li_3PS_7 (L3PS) catholyte in an electronically conductive carbon matrix, enabling high and balanced electronic/ionic conductivities in the cathode composite. The inherent porous structure of CMK-3 also helps to accommodate the strain/stress generated during the expansion and shrinkage of the active material. In sulfide-based all-solid-state batteries with Li metal as the anode, this cathode composite delivered a high capacity of 1025 mAh g^{-1} after 50 cycles at 60 °C at 1/8C. This work highlights the important role of high and balanced electronic and ionic conductivities in developing high-performance sulfur cathodes for ASSLSBs.

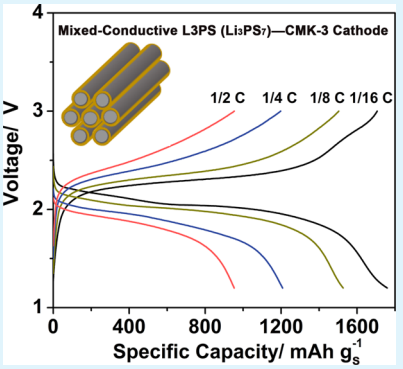

KEYWORDS: *sulfur cathode, mixed conductive, solid electrolyte, battery, composite*

INTRODUCTION

The ever-increasing demand on the energy density has posed a serious concern on the safety of today's lithium-ion batteries.[1,2] All-solid-state batteries using nonflammable solid electrolytes are being considered as a promising solution for safer batteries.[3−6] It is known that the maximum energy density of a solid-state battery is determined by the cathode composite for a fixed capacity ratio of negative to positive electrodes (N/P ratio) and a fixed amount of solid electrolyte. Sulfur, because of its high theoretical capacity, has received intense research interest as the cathode active material.[7−9] A recent analysis by Janek also pointed out that with a 50-μm-thick solid electrolyte, sulfur is the only cathode that can enable a solid-state battery with exceptionally high energy density beyond 500 Wh kg^{-1}.[10] Nevertheless, developing sulfur cathodes with a high performance in terms of sulfur utilization, cycle life, and rate performance is very challenging due to (i) the insulating nature of sulfur for both electrons and ions and (ii) the large volume change of sulfur (80%) during lithiation/delithiation.[11]

Inspired by the success of liquid-electrolyte Li–S batteries,[12] tremendous efforts have been done to improve the electronic conductivity of sulfur cathodes by introducing various electronically conductive additives such as copper,[13,14] acetylene black,[15] carbon nanofibers,[16] reduced graphene oxide,[17] and graphite.[18] However, the performance improvement in all-solid-state lithium–sulfur batteries (ASSLSBs) is not as effective as that in the liquid-electrolyte Li–S batteries. Such a difference is mainly caused by the different properties of solid electrolytes and liquid electrolytes. Unlike liquid electrolytes that are infiltrative and flowable, solid electrolytes are usually fixed at their positions once the cathode has been prepared. As a result, the ionic conduction percolation in the cathode composite is much harder to achieve in solid-state batteries than that in the liquid-electrolyte batteries. To improve the ionic conductivity of electrodes, several lithium superionic sulfides such as lithium polysulfidophosphate[19] and Li_3PS_4 (LPS)-coated Li_2S[20] were fabricated by Liang et al. as the cathodes for ASSLSBs. These superionic sulfides were then mixed with carbon and binder to make the mixed-conductive cathode composites. Despite apparent improvement in the cycling stability (>100 cycles), these superionic cathodes are usually tested with a low loading of active material (0.25–0.60 mg cm^{-2}).[19,20] One main reason for the limited performance improvement is that most of the above-mentioned work only focused on improving one conductivity at nanoscale, either electronic or ionic, in the cathode composite, while for an ideal cathode, both electronic and ionic conductivities should be

Received: May 10, 2020
Accepted: July 20, 2020
Published: July 20, 2020

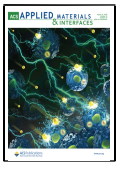

https://dx.doi.org/10.1021/acsami.0c08564
ACS Appl. Mater. Interfaces 2020, 12, 36066–36071

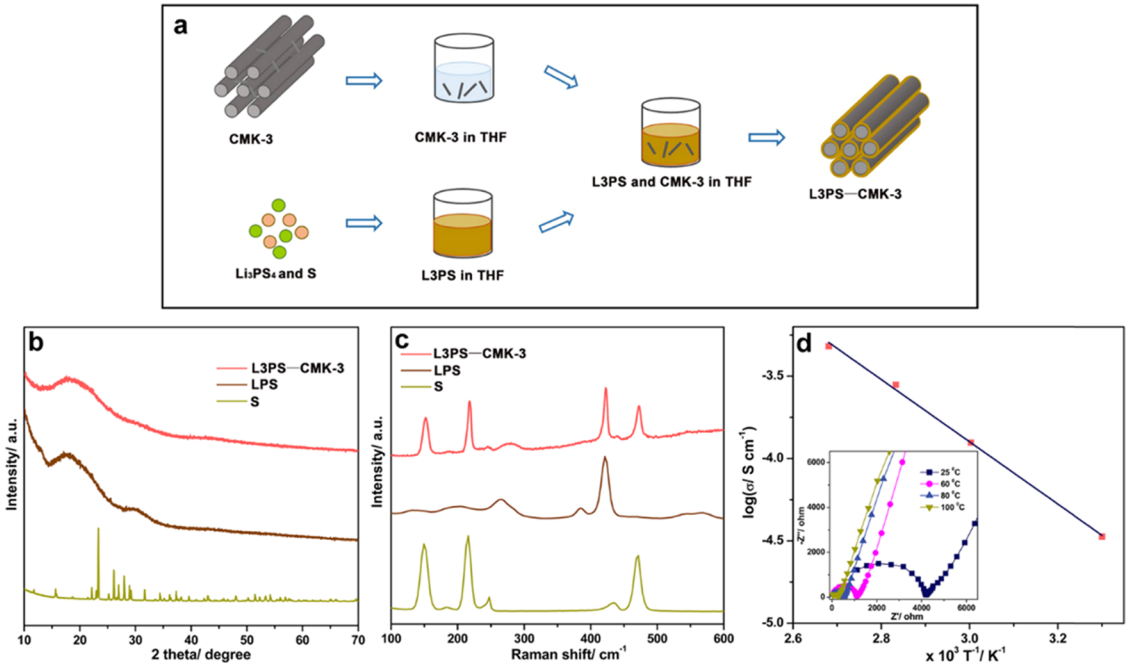

Figure 1. (a) Schematic synthesis process for the fabrication of the L3PS−CMK-3 composite. (b) XRD patterns and (c) Raman spectra of S, LPS, and L3PS−CMK-3. (d) Arrhenius plots and electrochemical impedance spectra at different temperatures (inset) of L3PS.

ensured at nanoscale for a high utilization of sulfur. In addition to this, the huge stress/strain caused by the volume change of sulfur during operation has not been addressed, which will certainly affect the performance improvement.[11,21,22]

In this work, we developed a nanoscale mix-conducive sulfur cathode for all-solid-state lithium batteries. By infiltrating a solution with highly ionic conductive Li_3PS_7 (L3PS) active material into mesoporous carbon CMK-3, we were able to fabricate a cathode with both high and balanced ionic and electronic conductivities and with an inherent porous structure to accommodate the volume change of active materials. The cathode composite exhibits excellent cycling and rate performance in an all-solid-state lithium battery even with no additional solid electrolyte and carbon added in the electrode.

EXPERIMENTAL SECTION

Material Synthesis. Li_3PS_4 glass solid electrolyte was prepared by a mechanical milling process. In brief, 75 mol % of lithium sulfide (Li_2S, Sigma-Aldrich) and 25 mol % of phosphorus pentasulfide (P_2S_5, Sigma-Aldrich) were mixed in a zirconia pot at a fixed rotation speed of 510 rpm for 45 h.[30] To prepare L3PS−CMK-3 composite, a mixture of 0.18 g of Li_3PS_4 glass solid electrolyte and 0.096 g of sulfur (S, Sigma-Aldrich) was dissolved in 6 mL of tetrahydrofura (THF, Sigma-Aldrich) solvent, while 0.096 g ordered mesoporous carbon (CMK-3, ACS Material) powders were dispersed in another 6 mL of THF solvent. After that, these two solutions were mixed together and stirred overnight. All of the above processes were conducted under argon. The mixed solution was then dried at 80 °C for 24 h under vacuum to completely remove the THF solvent, and the L3PS−CMK-3 composite was obtained. A composite of S, Li_3PS_4 glass solid electrolyte, and CMK-3 (demoted as 3S−LPS−CMK-3) with the same weight ratio was also prepared by a ball-milling method (370 rpm for 1 h) as a control sample.

Material Characterization. XRD patterns were obtained using a D8 Advance X-ray diffractometer (Bruker AXS, WI) with Cu Kα radiation. A 532 nm diode-pumped solid-state laser was used on a Horiba Jobin Yvon Labram Aramis to record Raman spectra. To characterize the morphologies of samples, transmission electron microscopy (TEM) images and scanning electron microscopy (SEM) images were examined with transmission electron microscopy (TEM, JEM 2100 LaB6) and scanning electron microscopy (SEM, Hitachi SU-70), separately. N_2 adsorption/desorption isotherms were measured with Micromeritics ASAP 2020 Porosimeter Test Station. Surface areas were calculated with the Brunauer−Emmett−Teller (BET) method, and pore volume distribution was obtained using the Barrett−Joyner−Halenda (BJH) equation.

Electrochemical Measurement. All-solid-state lithium−sulfur batteries were fabricated using Li_3PS_4 glass as the solid electrolyte, Li metal as the anode, and L3PS−CMK-3 or 3S−LPS−CMK-3 as the cathode composite. The ionic conductivities of L3PS at different temperatures were measured using an ion-blocking Pt/L3PS/Pt cell. The cell was fabricated by pressing 150 mg of L3PS powders into pellets, followed by sputtering of Pt. Then, electrochemical impedance spectra (EIS) were measured at different temperatures. To assemble all-solid-state lithium−sulfur batteries, 150 mg of Li_3PS_4 glass was put in a poly(tetrafluoroethylene) (PTFE) tank with a diameter of 1 cm, and 5 mg of the L3PS−CMK-3 composite or the 3S−LPS−CMK-3 composite was pressed on top of the solid electrolyte under 360 MPa. Then, lithium metal was attached directly on the other side of the solid electrolyte layer. All electrochemical performances including cycling properties and rate performances were tested using LAND CT-2001A battery cyclers within 1.2−3.0 V at 60 °C. EIS spectra of all-solid-state lithium−sulfur batteries were measured using Solartron workstation in a frequency range of 1 MHz to 0.1 Hz with a 20 mV AC amplitude.

RESULTS AND DISCUSSION

Figure 1a demonstrates the synthesis process for the L3PS−CMK-3 composite. First, CMK-3 powders were dispersed in the THF solvent, and LPS glass and S with a molar ratio of 1:3 were dissolved in another THF solvent. These two solutions were then mixed together and dried under vacuum to get the L3PS−CMK-3 composite. Figure 1b shows the X-ray diffraction (XRD) patterns of S, LPS glass, and L3PS−CMK-3 composite. The XRD pattern of L3PS−CMK-3 in Figure 1b indicates the amorphous structure of composite and no peaks for S can be observed, while the broad peak at around 18° that is observed in the XRD patterns of both LPS and L3PS−CMK-

https://dx.doi.org/10.1021/acsami.0c08564
ACS Appl. Mater. Interfaces 2020, 12, 36066−36071

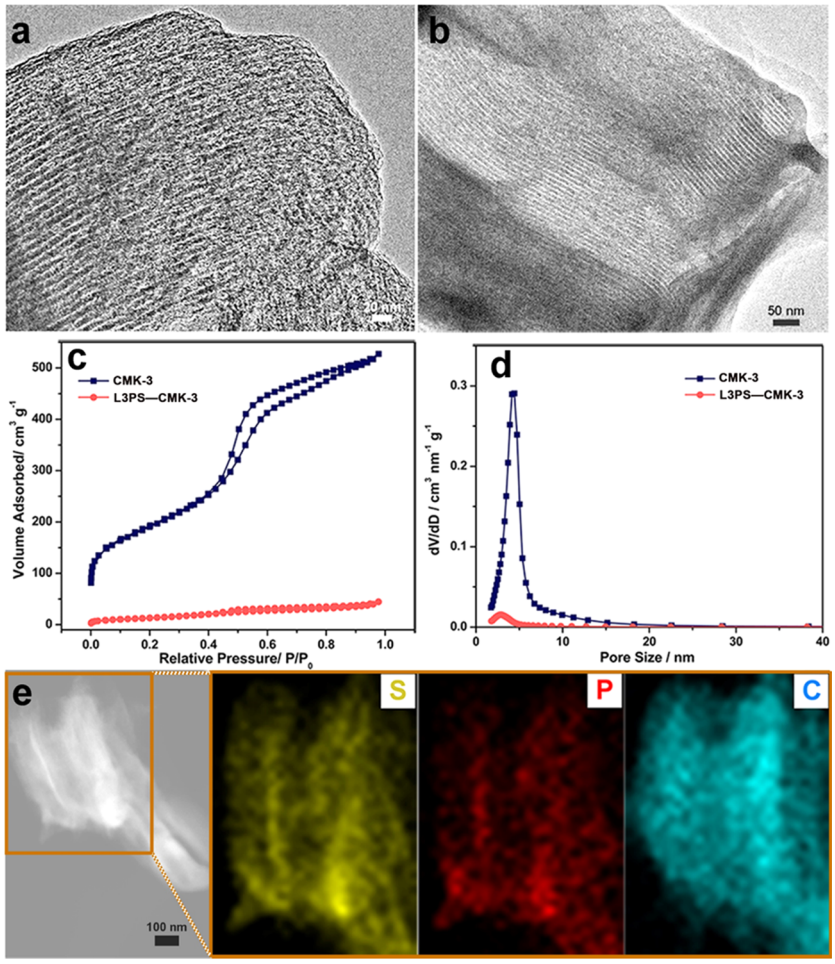

Figure 2. HRTEM images of (a) CMK-3 and (b) L3PS−CMK-3 composite. (c) N_2 adsorption/desorption isotherms and (d) BJH pore size distributions for CMK-3 and L3PS−CMK-3. (e) TEM image and corresponding elemental mappings of S, P, and C in the L3PS−CMK-3 composite.

3 is due to the sample holder for the measurement. The result shows that LPS has completely reacted with active S forming a single amorphous phase, consistent with the study by Liang et al.[19]

The Raman spectra of the L3PS−CMK-3 composite consist of chemical signatures of both LPS and S, implying that L3PS can be used as both a solid electrolyte and a cathode active material, i.e., a catholyte. The ionic conductivity of L3PS was also measured from the electrochemical impedance spectra of a Pt/L3PS/Pt cell at different temperatures. The Arrhenius plot and the impedance plot at different temperatures are shown in Figure 1d. The activation energy for L3PS is calculated to be 0.376 eV, and its ionic conductivity can reach 1.25×10^{-4} S cm^{-1} at 60 °C, which is close to the previous report.[19]

Figure 2a,b compares the high-resolution TEM (HRTEM) images of CMK-3 and L3PS−CMK-3 composite, respectively. While a clear channel structure can be observed in the HRTEM image of CMK-3, the channels seem to be filled after infiltrating with L3PS. The infiltration of L3PS inside the pores of CMK-3 is also supported by the reduced surface area (Figure 2c), and more importantly, by the reduced pore size (Figure 2d) of L3PS−CMK-3 when comparing with pure CMK-3. Figure 2e displays the elemental mappings in the L3PS−CMK-3 composite. A homogeneous distribution of S, P, and C can be easily observed in the composite, further confirming that L3PS was uniformly filled in the CMK-3 carbon matrix. The uniform distribution of L3PS in CMK-3 is also supported by the SEM images (Figure S1). A much more homogeneous distribution of S, P, and C can be observed in L3PS−CMK-3 than in the 3S−LPS−CMK-3 cathode composite prepared by ball-milling S, LPS, and CMK-3 with the same weight ratio as the SEM image and elemental mappings (Figure S2), TEM image (Figure S3) and XRD pattern (Figure S4 and S5) of 3S−LPS−CMK-3 indicate that it is mainly a composite of the three phases.

The electrochemical performances of L3PS−CMK-3 and 3S−LPS−CMK-3 composite cathodes were tested in all-solid-state lithium−sulfur batteries using LPS glass as the solid electrolyte and Li as the anode between 1.2 and 3 V at 60 °C. Figure 3a shows the charge−discharge profiles of L3PS−CMK-3 cathode at a current density of 1/8C (1C = 1675 mA g^{-1}). Only one plateau (2.0 V for the discharge process and 2.2 V for the charge process) can be observed, which is consistent with the binary (between Li_2S and S) phase transition during cycling,[19,23] although the reversible decomposition of solid electrolyte should also occur and contribute slightly to the capacity of the cathode composite.[24,25] Compared with the charge−discharge curves of the 3S−LPS−CMK-3 composite in Figure 3b, a higher specific capacity can be observed for the L3PS−CMK-3 cathode. Also, L3PS−CMK-3 exhibits smaller overpotentials than the 3S−LPS−CMK-3 composite cathode, especially after more than three cycles, indicating better

https://dx.doi.org/10.1021/acsami.0c08564
ACS Appl. Mater. Interfaces 2020, 12, 36066−36071

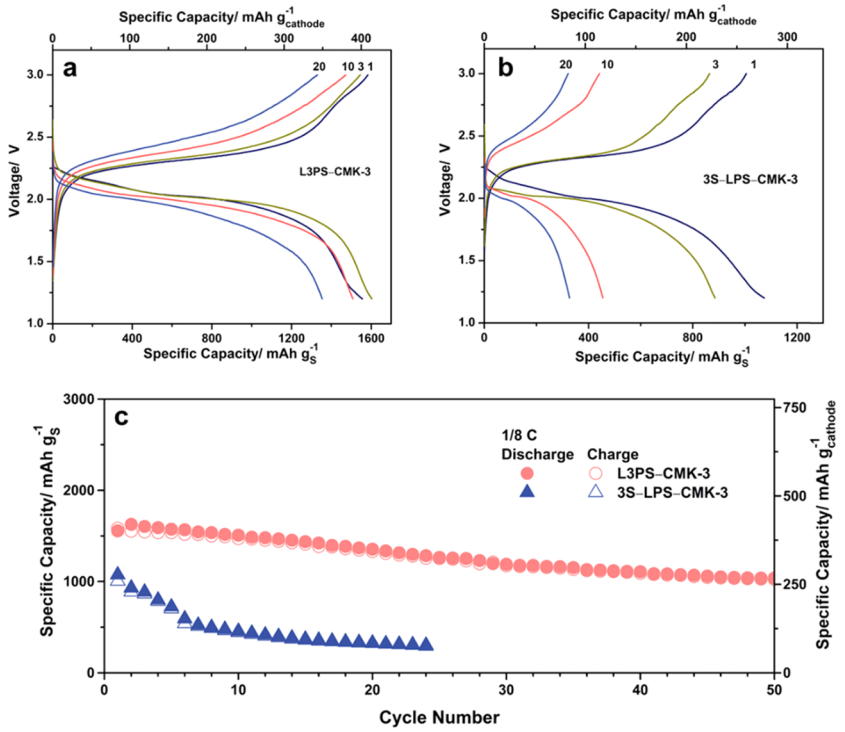

Figure 3. Electrochemical performances of L3PS−CMK-3 and 3S−LPS−CMK-3 composites in all-solid-state lithium−sulfur batteries at 60 °C between 1.2 and 3.0 V. The specific capacities were calculated based on the weight of sulfur and the total weight of the cathode composite. Charge−discharge curves at different cycles for (a) L3PS−CMK-3 and (b) 3S−LPS−CMK-3 composite cathodes at a current density of 1/8C (1C = 1675 mA g^{-1}). (c) Cycling performances of L3PS−CMK-3 and 3S−LPS−CMK-3 composite cathodes at a current density of 1/8C.

kinetics in the L3PS−CMK-3 composite. Correspondingly, much better cycling stability for the L3PS−CMK-3 composite can be obviously observed in Figure 3c. At the current density of 1/8C, the 3S−LPS−CMK-3 composite presents a reversible specific capacity of 1004 mAh g^{-1} in the first cycle, and the capacity quickly decays to 322 mAh g^{-1}within 20 cycles. However, the L3PS−CMK-3 composite delivers a much higher reversible specific capacity of 1583 mAh g^{-1} in the first cycle, and the specific capacity maintains 1025 mAh g^{-1} after 50 cycles. No apparent segregation of active material can be observed in the cathode composite (Figure S6), indicating the excellent stability of L3PS−CMK-3 during charge and discharge processes. In addition, we also tested the performance of the cathode with the higher S content. Figure S7 shows the charge/discharge curves and cycling performances of L3PS−CMK-3, L3.67PS−CMK-3, and L4.33PS−CMK-3, where L3PS, L3.67PS, and L4.33PS correspond to the molar ratio of 1:3, 1:4, and 1:5 between Li_3PS_4 and S. L3PS−CMK-3 shows much higher capacities than L3.67PS−CMK-3 and L4.33PS−CMK-3 over 50 cycles probably due to a well-balanced electronic conductivity and ionic conductivity and therefore is selected in this work. It should be noted that the S content in the L3PS−CMK-3 cathode is comparable with or even higher than the previous reports,[15,26−29] highlighting the important role of high and balanced electronic and ionic conductivities in developing the S cathode composite.

Figure 4 shows the impedance plots of all-solid-state batteries using L3PS−CMK-3 and 3S−LPS−CMK-3 composites as the cathodes. Each EIS curve consists of one semicircle in the high-frequency region and one slope in the low-frequency region. The semicircle corresponds to the interfacial resistance from the anode/electrolyte interface and the cathode/electrolyte interface. Since all anodes are the same

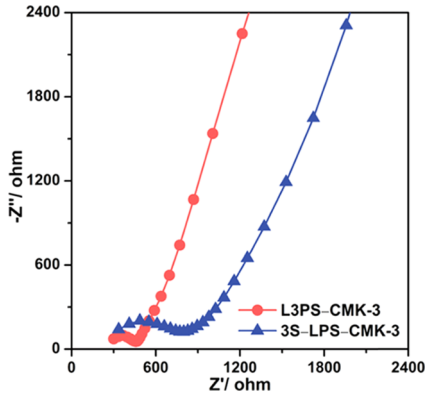

Figure 4. Electrochemical impedance spectra for the all-solid-state Li cells using L3PS−CMK-3 and 3S−LPS−CMK-3 composites as the cathodes. Both cells were fully discharged and charged for three cycles prior to the EIS test.

anode, the difference in the interfacial resistance of these two cells could be mainly attributed to the interfacial resistance between the cathode and solid electrolyte. The result demonstrates a much better kinetics of the L3PS−CMK-3 composite than that of the 3S−LPS−CMK-3 composite. Since we are using exactly the same active material, solid electrolyte, and electronic conductive additive with exactly the same weight ratio in the two cathodes, the enhanced kinetics is mainly caused by higher conductivities (both electronic and ionic) due to a more uniform distribution of active material, ionic conductive material, and electronic conductive material at the nanoscale in the L3PS−CMK-3 composite, as is supported by the higher conductivity of a single-phase L3PS than that of a 3S−LPS composite (Figure S8).

https://dx.doi.org/10.1021/acsami.0c08564
ACS Appl. Mater. Interfaces 2020, 12, 36066−36071

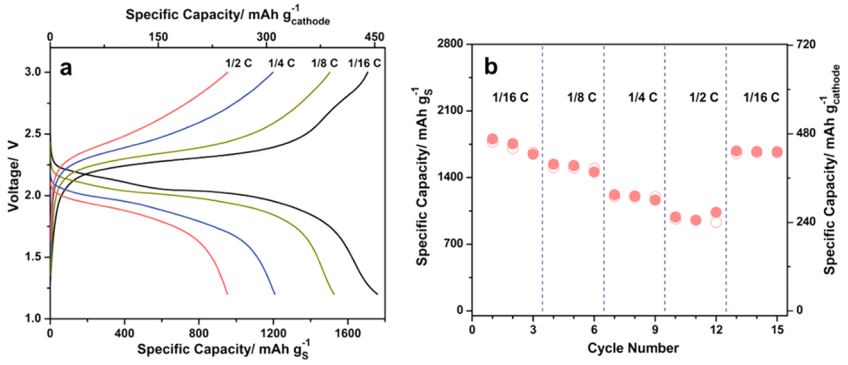

Figure 5. (a) Charge−discharge curves of the L3PS−CMK-3 cathode composite at different current densities and (b) corresponding rate performance of the L3PS−CMK-3 cathode composite. The specific capacities were calculated based on the weight of sulfur and the total weight of the cathode composite. These cells were discharged and charged at various current densities from 1/16C to 1/2C at 60 °C between 1.2 and 3.0 V.

We then tested the rate performance of the L3PS−CMK-3 composite cathode between 1.2 and 3 V at 60 °C. The cell was cycled at various current densities from 1/16C to 1/2C. At each current density, the cell was discharged and charged for three cycles. Charge−discharge curves at different current densities are given in Figure 5a, and the rate capacity is shown in Figure 5b. The L3PS−CMK-3 cathode could deliver reversible capacities of 1759, 1527, 1208, and 953 mAh g^{-1} at current densities of 1/16C (0.18 mA cm^{-2}), 1/8C (0.35 mA cm^{-2}), 1/4C (0.69 mA cm^{-2}), and 1/2C (1.38 mA cm^{-2}), respectively. Therefore, the L3PS−CMK-3 composite also presents excellent rate performance even though no additional solid electrolyte and carbon were added in the electrode. The high utilization of S and excellent rate performance can be ascribed to the uniform distribution of active material, solid electrolyte, and carbon, which leads to high and balanced ionic and electronic conductivities in the cathode composites. Additionally, the inherent porous structure of CMK-3 can also buffer the volume change generated during charge−discharge processes, which helps improve the cycling stability.

CONCLUSIONS

In summary, a mixed-conductive composite of L3PS−CMK-3 was prepared by infiltrating L3PS (chemical composition: Li_3PS_7) catholyte into mesoporous CMK-3. This approach results in intimate contacts between active material, solid electrolyte, and carbon and thus leads to a high and balanced mixed conductivity in the cathode composite. In addition, the porous carbon matrix can accommodate the strain/stress during cycling. The cathode composite exhibited excellent cycling stability (1025 mAh g^{-1} after 50 cycles) and rate performance up to 1/2C in all-solid-state lithium−sulfur battery at 60 °C. While the rate performance of the cathode has been improved largely due to the enhanced ionic and electronic conductivities, the cycling performance of the mixed-conductive cathode is still limited. Further work is needed to understand more about the degradation mechanism of this cathode composite.

ASSOCIATED CONTENT

Supporting Information

The Supporting Information is available free of charge at https://pubs.acs.org/doi/10.1021/acsami.0c08564.

SEM images and corresponding elemental mappings for the L3PS−CMK-3 composite; SEM image and elemental mappings, TEM image, and XRD pattern of the 3S−LPS−CMK-3 composite; XRD patterns of 3S−LPS and L3PS; SEM image and elemental mappings of 3S−LPS−CMK-3 after charging and discharging; electrochemical performance of cathode composites with different molar ratios between Li3PS4 and S during synthesis; ionic conductivities of 3S−LPS and L3PS (PDF)

AUTHOR INFORMATION

Corresponding Authors

Fudong Han − *Department of Mechanical, Aerospace, and Nuclear Engineering, Rensselaer Polytechnic Institute, Troy, New York 12180, United States;* orcid.org/0000-0003-2507-4340; Email: hanf2@rpi.edu

Chunsheng Wang − *Department of Chemical and Biomolecular Engineering, University of Maryland, College Park, Maryland 20742, United States;* orcid.org/0000-0002-8626-6381; Email: cswang@umd.edu

Authors

Jie Yue − *Department of Chemical and Biomolecular Engineering, University of Maryland, College Park, Maryland 20742, United States*

Yonglin Huang − *Department of Mechanical, Aerospace, and Nuclear Engineering, Rensselaer Polytechnic Institute, Troy, New York 12180, United States*

Sufu Liu − *Department of Chemical and Biomolecular Engineering, University of Maryland, College Park, Maryland 20742, United States*

Ji Chen − *Department of Chemical and Biomolecular Engineering, University of Maryland, College Park, Maryland 20742, United States;* orcid.org/0000-0003-0326-8304

Complete contact information is available at: https://pubs.acs.org/10.1021/acsami.0c08564

Notes

The authors declare no competing financial interest.

ACKNOWLEDGMENTS

C.W. and F.H. gratefully acknowledge support by the National Science Foundation (Award No. 1805159) and the U.S. Department of Energy ARPA-E (Award No. DE-AR0000781).

REFERENCES

(1) Janek, J.; Zeier, W. G. A. Solid Future for Battery Development. *Nat. Energy* **2016**, *1*, No. 16141.

(2) Robinson, A. L.; Whittingham, M. S. Pushing the Frontiers of Lithium-Ion Batteries Raises Safety Questions. *MRS Bull.* **2016**, *41*, 188−189.
(3) Schnell, J.; Gunther, T.; Knoche, T.; Vieider, C.; Kohler, L.; Just, A.; Keller, M.; Passerini, S.; Reinhart, G. All-Solid-State Lithium-Ion and Lithium Metal Batteries - Paving the Way to Large-Scale Production. *J. Power Sources* **2018**, *382*, 160−175.
(4) Mauger, A.; Armand, M.; Julien, C. M.; Zaghib, K. Challenges and Issues Facing Lithium Metal for Solid-State Rechargeable Batteries. *J. Power Sources* **2017**, *353*, 333−342.
(5) Hayashi, A.; Sakuda, A.; Tatsumisago, M. Development of Sulfide Solid Electrolytes and Interface Formation Processes for Bulk-Type All-Solid-State Li and Na Batteries. *Front. Energy Res.* **2016**, *4*, No. 25.
(6) Luntz, A. C.; Voss, J.; Reuter, K. Interfacial Challenges in Solid-State Li Ion Batteries. *J. Phys. Chem. Lett.* **2015**, *6*, 4599−4604.
(7) McCloskey, B. D. Attainable Gravimetric and Volumetric Energy Density of Li−S and Li Ion Battery Cells with Solid Separator-Protected Li Metal Anodes. *J. Phys. Chem. Lett.* **2015**, *6*, 4581−4588.
(8) Betz, J.; Bieker, G.; Meister, P.; Placke, T.; Winter, M.; Schmuch, R. Theoretical Versus Practical Energy: A Plea for More Transparency in the Energy Calculation of Different Rechargeable Battery Systems. *Adv. Energy Mater.* **2019**, *9*, No. 1900761.
(9) Yan, M.; Wang, W.-P.; Yin, Y.-X.; Wan, L.-J.; Guo, Y.-G. Interfacial Design for Lithium-Sulfur Batteries: from Liquid to Solid. *EnergyChem* **2019**, *1*, No. 100002.
(10) Randau, S.; Weber, D. A.; Kotz, O.; Koerver, R.; Braun, P.; Weber, A.; Ivers-Tiffee, E.; Adermann, T.; Kulisch, J.; Zeier, W. G.; Richter, F. H.; Janek, J. Benchmarking the Performance of All-Solid-State Lithium Batteries. *Nat. Energy* **2020**, *5*, 259−270.
(11) Barai, P.; Mistry, A.; Mukherjee, P. P. Poromechanical Effect in the Lithium−Sulfur Battery Cathode. *Extreme Mech. Lett.* **2016**, *9*, 359−370.
(12) Ji, X.; Lee, K. T.; Nazar, L. F. A Highly Ordered Nanostructured Carbon-Sulphur Cathode for Lithium-Sulphur Batteries. *Nat. Mater.* **2009**, *8*, 500−506.
(13) Hayashi, A.; Ohtsubo, R.; Tatsumisago, M. Electrochemical Performance of All-Solid-State Lithium Batteries with Mechanochemically Activated Li_2S−Cu Composite Electrodes. *Solid State Ionics* **2008**, *179*, 1702−1705.
(14) Hayashi, A.; Ohtomo, T.; Mizuno, F.; Tadanaga, K.; Tatsumisago, M. All-Solid-State Li/S Batteries with Highly Conductive Glass−Ceramic Electrolytes. *Electrochem. Commun.* **2003**, *5*, 701−705.
(15) Kobayashi, T.; Imade, Y.; Shishihara, D.; Homma, K.; Nagao, M.; Watanabe, R.; Yokoi, T.; Yamada, A.; Kanno, R.; Tatsumi, T. All Solid-State Battery with Sulfur Electrode and thio-LISICON Electrolyte. *J. Power Sources* **2008**, *182*, 621−625.
(16) Yamada, T.; Ito, S.; Omoda, R.; Watanabe, T.; Aihara, Y.; Agostini, M.; Ulissi, U.; Hassoun, J.; Scrosati, B. All Solid-State Lithium−Sulfur Battery Using a Glass-Type P_2S_5−Li_2S Electrolyte: Benefits on Anode Kinetics. *J. Electrochem. Soc.* **2015**, *162*, No. A646.
(17) Yao, X. Y.; Huang, N.; Han, F. D.; Zhang, Q.; Wan, H. L.; Mwizerwa, J. P.; Wang, C. S.; Xu, X. X. High-Performance All-Solid-State Lithium-Sulfur Batteries Enabled by Amorphous Sulfur-Coated Reduced Graphene Oxide Cathodes. *Adv. Energy Mater.* **2017**, *7*, No. 1602923.
(18) Agostini, M.; Aihara, Y.; Yamada, T.; Scrosati, B.; Hassoun, J. A Lithium−Sulfur Battery Using a Solid, Glass-Type P_2S_5−Li_2S electrolyte. *Solid State Ionics* **2013**, *244*, 48−51.
(19) Lin, Z.; Liu, Z.; Fu, W.; Dudney, N. J.; Liang, C. Lithium Polysulfidophosphates: A Family of Lithium-Conducting Sulfur-Rich Compounds for Lithium-Sulfur Batteries. *Angew. Chem., Int. Ed.* **2013**, *52*, 7460−7463.
(20) Lin, Z.; Liu, Z.; Dudney, N. J.; Liang, C. Lithium Superionic Sulfide Cathode for All-Solid Lithium−Sulfur Batteries. *ACS Nano* **2013**, *7*, 2829−2833.
(21) Zheng, M.; Tang, H.; Li, L.; Hu, Q.; Zhang, L.; Xue, H.; Pang, H. Hierarchically Nanostructured Transition Metal Oxides for Lithium-Ion Batteries. *Adv. Sci.* **2018**, *5*, No. 1700592.
(22) Li, B.; Gu, P.; Zhang, G.; Lu, Y.; Huang, K.; Xue, H.; Pang, H. Ultrathin Nanosheet Assembled $Sn_{0.91}Co_{0.19}S_2$ Nanocages with Exposed (100) Facets for High-Performance Lithium-Ion Batteries. *Small* **2018**, *14*, No. 1702184.
(23) Han, F.; Yue, J.; Fan, X.; Gao, T.; Luo, C.; Ma, Z.; Suo, L.; Wang, C. High-Performance All-Solid-State Lithium-Sulfur Battery Enabled by a Mixed-Conductive Li_2S Nanocomposite. *Nano Lett.* **2016**, *16*, 4521−4527.
(24) Yue, J.; Han, F. D.; Fan, X. L.; Zhu, X. Y.; Ma, Z. H.; Yang, J.; Wang, C. S. High-Performance All-Inorganic Solid-State Sodium-Sulfur Battery. *ACS Nano* **2017**, *11*, 4885−4891.
(25) Richards, W. D.; Miara, L. J.; Wang, Y.; Kim, J. C.; Ceder, G. Interface Stability in Solid-State Batteries. *Chem. Mater.* **2016**, *28*, 266−273.
(26) Suzuki, K.; Sakuma, M.; Hori, S.; Nakazawa, T.; Nagao, M.; Yonemura, M.; Hirayama, M.; Kanno, R. Synthesis, Structure, and Electrochemical Properties of Crystalline Li-P-S-O Solid Electrolytes: Novel Lithium-Conducting Oxysulfides of $Li_{10}GeP_2S_{12}$ Family. *Solid State Ionics* **2016**, *288*, 229−234.
(27) Nagao, M.; Suzuki, K.; Imade, Y.; Tateishi, M.; Watanabe, R.; Yokoi, T.; Hirayama, M.; Tatsumi, T.; Kanno, R. All-Solid-State Lithium-Sulfur Batteries with Three-Dimensional Mesoporous Electrode Structures. *J. Power Sources* **2016**, *330*, 120−126.
(28) Suzuki, K.; Kato, D.; Hara, K.; Yano, T. A.; Hirayama, M.; Hara, M.; Kanno, R. Composite Sulfur Electrode Prepared by High-Temperature Mechanical Milling for Use in an All-Solid-State Lithium-Sulfur Battery with a $Li_{3.25}Ge_{0.25}P_{0.75}S_4$ Electrolyte. *Electrochim. Acta* **2017**, *258*, 110−115.
(29) Trevey, J. E.; Gilsdorf, J. R.; Stoldt, C. R.; Lee, S. H.; Liu, P. Electrochemical Investigation of All-Solid-State Lithium Batteries with a High Capacity Sulfur-Based Electrode. *J. Electrochem. Soc.* **2012**, *159*, A1019−A1022.
(30) Tsukasaki, H.; Mori, Y.; Otoyama, M.; Yubuchi, S.; Asano, T.; Tanaka, Y.; Ohno, T.; Mori, S.; Hayashi, A.; Tatsumisago, M. Crystallization Behavior of the Li_2S-P_2S_5 Glass Electrolyte in the $LiNi_{1/3}Mn_{1/3}Co_{1/3}O_2$ Positive Electrode Layer. *Sci. Rep.* **2018**, *8*, No. 6214.

https://dx.doi.org/10.1021/acsami.0c08564
ACS Appl. Mater. Interfaces 2020, 12, 36066−36071